Small Methods

Imaging of Unstained DNA Origami Triangles with Electron Microscopy

--Manuscript Draft--

Manuscript Number:	
Full Title:	Imaging of Unstained DNA Origami Triangles with Electron Microscopy
Article Type:	Communication
Section/Category:	
Keywords:	
Corresponding Author:	Tanya Prozorov, Ph.D. US DOE Ames Laboratory Ames, IA UNITED STATES
Corresponding Author Secondary Information:	
Corresponding Author's Institution:	US DOE Ames Laboratory
Corresponding Author's Secondary Institution:	
First Author:	Tanya Prozorov, Ph.D.
First Author Secondary Information:	
Order of Authors:	Tanya Prozorov, Ph.D.
	Alejandra Londono-Calderon
	Md Mir Hossen
	Pierre E. Palo
	Lee Bendickson
	Sandra Vergara
	Marit Nilsen-Hamilton, Ph.D.
	Andrew C. Hillier, Ph.D.
Order of Authors Secondary Information:	
Additional Information:	
Question	**Response**
Please submit a plain text version of your cover letter here.	May 26, 2019 Dear Editors, We are delighted to submit a revised manuscript entitled “Imaging of Unstained DNA Origami Triangles with Electron Microscopy” to Small Methods. Characterization of scaffolded DNA and DNA origami nanostructures has been long dominated by atomic force microscopy, with the majority of electron microscopy imaging DNA origami, comprised of light elements, reporting either on the use of negative staining agents or utilizes cryo-TEM imaging, each relying on specific preparatory protocols and often prone to artifacts. Our manuscript describes direct imaging of visibly intact DNA origami nanostructures with high angular annular dark field scanning transmission electron microscopy (HAADF-STEM). We present here proof-of-concept results demonstrating that electron microscopy can be utilized to resolve key elements of the DNA origami triangle, without staining or employing

	exceedingly complicated preparation protocols. We monitored integrity of DNA origami triangles and demonstrated that these nanostructures were preserved and visualized without introducing artefacts or distortions associated with preparatory procedures. Our approach is suitable for depositing and imaging of DNA triangles with mass-thickness contrast sufficient to identify the scaffold-to-scaffold distances and the length of the triangle's seam on three supported carbon TEM grids, commercially available and widely used by the researchers. We show signal-to-noise ratio (SNR) of the DNA supported on amorphous carbon film as a function of the carbon thickness to analyze the image resolution, permitting edge detection of thin DNA triangles on substantially thicker carbon substrates. We discuss using cationic pre-treatment of the amorphous carbon grids with MgCl2 prior to DNA origami deposition and associated SNR image enhancement as an alternative approach to using a buffer with high cation concentration in suspensions. We also show the comparison between divalent and monovalent cations used in grid pre-treatment and discuss our findings in terms of effect of atomic number and valence of the cation on the contrast enhancement. We expect our findings will be widely used by researchers working in the field of DNA characterization, offering a straightforward method to high resolution imaging of these nanostructures. We envision this to be an important milestone in development of EM based imaging methods toward comprehensive DNA origami characterization utilizing capabilities afforded by the analytical spectroscopy. The attached manuscript is an estimated 6500 words long, including 6 Figures and 3 Tables. Supplementary Information providing additional details regarding DNA origami deposition, characterization and imaging is also included. A set of suggested expert reviewers is provided below. We look forward to your evaluation of our submission. We believe that we have addressed all of the concerns of the Reviewers and hope that the amended manuscript is appropriate for acceptance for publication. Yours sincerely, Tanya Prozorov, Ph.D. Division of Materials Sciences and Engineering US DOE Ames Laboratory 332 Wilhelm Hall, 2332 Pammel Drive Ames IA 50011 e-mail: tprozoro@ameslab.gov Suggested expert reviewers: 1)Damien Alloyeau, CNRS Universite Paris Diderot, e-mail: damien.alloyeau@univ-paris-diderot.fr 2)Yoones Kabiri, Kavli Institute of Nanoscience Delft, Delft University of Technology: e-mail: y.kabiri@tudelft.nl 3)Mario Ancona, U.S. Naval Research Laboratory, e-mail: mario.ancona@nrl.navy.mil 4)Oleg Gang, Columbia University: e-mail: og2226@columbia.edu 5)Mauri A. Kostiainen, Aalto University School of Chemical Technology, e-mail: mauri.kostiainen@aalto.fi 6)Enzo Di Fabrizio, King Abdullah University of Science and Technology, e-mail: enzo.difabrizio@kaust.edu.sa 7)Adrian Keller, Universität Paderborn, e-mail: adrian.keller@upb.de
Do you or any of your co-authors have a conflict of interest to declare?	No. The authors declare no conflict of interest.

WILEY-VCH

Imaging of Unstained DNA Origami Triangles with Electron Microscopy

*Alejandra Londono-Calderon, Md Mir Hossen, Pierre E. Palo, Lee Bendickson, Sandra Vergara, Marit Nilsen-Hamilton, Andrew C. Hillier and Tanya Prozorov**

Dr. A. Londono-Calderon, Dr. T. Prozorov*

US DOE Ames Laboratory, Division of Materials Science and Engineering, Ames, IA 50011, USA.

E-mail: tprozoro@ameslab.gov

M. M. Hossen, Prof. A. C. Hillier

Iowa State University, Department of Chemical and Biological Engineering, Ames, IA 50011, USA.

US DOE Ames Laboratory, Division of Materials Science and Engineering, Ames, IA 50011, USA.

Dr. P. E. Palo, L. Bendickson, Prof. M. Nilsen-Hamilton

Iowa State University, Roy J. Carver Department of Biochemistry, Biophysics and Molecular Biology, Ames, IA 50011, USA.

US DOE Ames Laboratory, Division of Materials Science and Engineering, Ames, IA 50011, USA.

Dr. S. Vergara

University of Pittsburgh, Department of Structural Biology, Pittsburgh, PA, 15261, USA.

Keywords: DNA origami, unstained DNA, Atomic Force Microscopy, Scanning Transmission Electron Microscopy, Signal-to-Noise Ratio,

Imaging of scaffolded DNA and DNA origami nanostructures has been dominated by atomic force microscopy of samples immobilized on bulk substrates. Less commonly used for DNA imaging are electron microscopy techniques, which are typically carried out either after negative staining of DNA or by direct imaging using a bright field cryo-TEM. Here, direct imaging of unstained DNA origami nanostructures on thin electron-transparent substrates utilizing high angular annular dark field scanning transmission electron microscopy (HAADF-STEM) is reported. This approach establishes a simple method for depositing and imaging intact DNA triangles with mass-thickness contrast, sufficient to measure the scaffold-to-scaffold distances and the length of the triangle's seam. The signal-to-noise ratio (SNR) of the DNA supported on amorphous carbon as a function of the carbon thickness is measured on three types of commercially available TEM grids to analyze the image resolution. This allows for an edge detection of ~1 nm height DNA triangles on carbon substrates as thick as ~25 nm. Additional observations on the effect on SNR with the imaging modes are discussed. The effect of cation concentration used for pre-treating the grid surface on the image resolution is also explored. Our work presents *proof-of-concept* results demonstrating that electron microscopy can be utilized to resolve key elements of the DNA origami triangle, without staining or employing exceedingly complicated preparation protocols.

1. Introduction

The use of scaffolded DNA origami shapes offers a flexible pathway for creating molecular building blocks with potential applications in biomedicine,[1] sensing,[2] fabrication of plasmonic nanostructures,[3] among others.[4] The complementarity of DNA allows the design of customized sequences for fabricating two- and three-dimensional nanostructures with nanometer

precision by molecular self-assembly.[5] These methods can be expanded to create functional devices similar to those achieved by top-down techniques.[6] High-resolution imaging of DNA and DNA-based origami nanostructure has long been dominated by atomic force microscopy (AFM). The resolution of the AFM imaging is influenced by the nature of the sample, the environmental conditions in which AFM is performed (liquid or dry medium), the mode of imaging (contact or non-contact) and, most importantly, the sharpness or the radius of the tip used for imaging.[7] Due to the curvature of the probe, the lateral resolution is lower than the vertical resolution. Conventional AFM tips with a radius of curvature in the ~20 nm range are expected to exhibit a lateral resolution on the order of 5-6 nm.[8] While state-of-the-art AFM instruments allow direct visualization of the scaffold, some of the drawbacks of this technique are associated with the to tip effects and an inherent incompatibility with concurrent localized analytical spectroscopy measurements. Electron microscopy (EM) imaging can potentially resolve sub-nanometer features of nucleic acids and provide localized chemical information by employing advanced analytical spectroscopy techniques, such as energy-dispersive X-ray spectroscopy (EDS), electron energy loss spectroscopy (EELS) and energy filtering transmission electron microscopy (EFTEM).[9] However, EM imaging of DNA nanostructures is challenging due to the low contrast associated with the chemical composition and the low electron density of these materials. Additional challenges for both AFM and EM imaging techniques are related to the necessity of immobilizing DNA on ultra-flat and electron transparent substrates, respectively. Spreading methods have been most frequently used to adhere nucleic acids to pretreated surfaces for electron microscopy imaging. Divalent cation-assisted treatment of mica with magnesium ions was first proposed for EM characterization of DNA,[10] as a method to increase the affinity of the DNA molecule to the substrate, and later used by Bustamante *et al.*[11] for reliable AFM

analysis of plasmid DNA. The popularity of this method has been extended to include a variety of substrates[12] and additional divalent metal cations.[13]

Direct transmission electron microscopy (TEM) imaging of DNA is typically limited to either cryo-EM analysis,[14] which employs a complex preparation protocol and low dose imaging, or negative staining to enhance image contrast.[15] Only recently, unstained double-stranded DNA has been successfully imaged with TEM using DNA fibers stretched between Si pillars.[16] In his pioneering work, Rothemund introduced the technique of DNA origami by using a DNA scaffold combined with short staples for creating three dimensional nanostructures that can reach hundreds of nanometers in size.[17] This led to an increased interest in the use of electron microscopy for detailed imaging of unique shapes afforded by these nanostructures. However, very few papers describe protocols for depositing and imaging of DNA origami nanostructures on electron-transparent substrates [9a, 18] without resorting to the use of cryo-EM or negative staining techniques. EM imaging of unstained DNA origami nanostructures is typically susceptible to size and shape distortion when immobilized on graphene[18a] or amorphous carbon[9a]. Currently, reports are lacking standardized protocols suitable for imaging of visibly intact DNA origami nanostructures with high angular annular dark field scanning transmission electron microscopy (HAADF-STEM) capable of providing sufficient contrast and resolution to access fine details of these nanostructures, without the use of contrast-enhancing negative staining agents.

Here, we present an approach to imaging of DNA origami nanostructures with electron microscopy while keeping the DNA structure visibly intact, without applying negative staining agents. Our approach utilizes positively charged divalent cations, which increases the affinity between the negatively charged amorphous carbon substrate and the DNA, as well as improves

image contrast.[8, 19] Our HAADF-STEM results are in good agreement with the shape and size of the designed DNA origami nanostructures and those determined by AFM.[12a] We show the effect of substrate thickness on the EM imaging resolution for three types of commercially available carbon film grids. We demonstrate that this approach to imaging DNA nanostructures can be used with both HAADF-STEM and conventional bright field (BF) TEM modes. We use the signal-to-noise ratio (SNR) of the acquired EM images to determine the optimal conditions for deposition and direct visualization of DNA origami nanostructures on amorphous carbon supports.

2. Results and Discussion

Imaging of DNA origami-shaped nanostructures is typically done after allowing the DNA deposited from a suspension to adhere to a substrate. Amorphous carbon films can be treated similarly to AFM suitable substrates to promote DNA adhesion, while providing an electron transparent surface for EM characterization. In this work, DNA sharp-edged origami triangles were chosen as model system because these shapes have been extensively imaged with AFM.[12a, b, 17, 20] **Figure 1(a)** shows typical AFM images of DNA origami triangles deposited from TAEM-1 buffer on mica (see methods for details).

The ultra-flatness and inherently negative surface charge of mica are well known to contribute to high-quality AFM images with minimal preparation protocols. Silicon substrates are also suitable for DNA deposition and imaging after aggressive plasma-cleaning.[21] Using the same DNA suspension, a weaker binding of the DNA to Si and SiO_2 substrates, compared to that of mica, has been reported in the presence of low-ionic strength buffer (TAEM1). Enhanced adherence of the DNA triangles to the Si surface was observed by increasing the TAE-Mg^{2+}

buffer concentration by a factor of ~10.[12b] **Figure 1(b)** shows adequate adhesion of DNA origami nanostructures to n-type Si after depositing a suspension of DNA triangles in 10×TAE-Mg^{2+} buffer on a plasma-treated Si substrate for five minutes (see **Methods** for details). Such an adhesion is believed to be mediated by the positively charged divalent Mg^{2+} cations having a strong ionic attraction to both the partially negatively-charged substrate and the DNA.[8, 19]

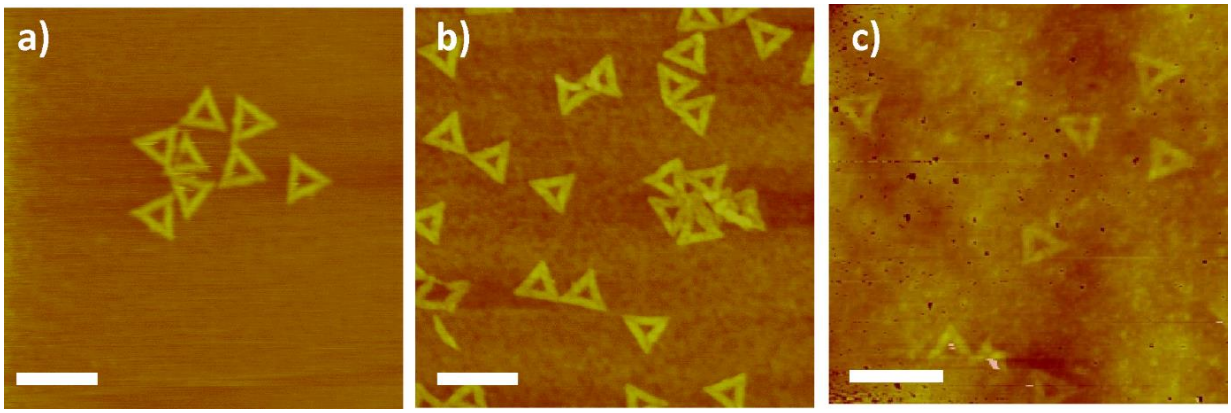

Figure 1. AFM images of DNA origami triangle nanostructures on **(a)** mica, and **(b)** silicon. A similar approach can be used for AFM imaging of DNA origami triangles deposited on thin electron transparent substrates, such as **(c)** ultrathin amorphous carbon film on a lacey carbon supported Cu TEM grid. Scale bar: 200 nm.

Negatively charged amorphous carbon-based electron transparent substrates could also provide a similar active surface for immobilization of DNA *via* magnesium salt bridges. UV-ozone plasma treatment was used to induce a negative charge on the surface of ultrathin (UT) amorphous carbon films supported by a lacey carbon film Cu TEM grid. **Figure 1(c)** shows AFM images of DNA origami triangles adhered to an UT carbon film on a lacey carbon Cu grid. Preparation of carbon grids and DNA deposition was carried out in a manner similar to that of the Si substrates, as described in the methods section. The measured roughness of mica, silicon and UT amorphous carbon represented by the Root Mean Square (RMS) values is shown in **Figure S1.** Discussion of substrate roughness and AFM imaging of DNA immobilized on a UT carbon film on a lacey carbon supported grid is presented in supporting information **Figure S2**.

Several attempts were made to improve the contrast of HAADF-STEM images of the DNA origami triangles. To enhance the DNA origami triangle density and contrast, a 10×TAE buffer with 12.5-125 mM Mg^{2+} was tested (buffers TAEM 1-4 as described in **Methods** section). The addition of Mg^{2+} cations to the suspension of DNA in the form of $MgCl_2$ was shown to increase significantly the image contrast. We also found that a suspension of 10-50 ng/μL DNA origami triangles ($13 - 67 \times 10^8$ nanostructures/μL) provided sufficient density of triangles on a carbon film without their overpopulating the area of the grid for EM characterization. **Figure 2(a)** shows an example of a low magnification HAADF-STEM image (*M = 225,000x*) of a group of DNA triangles on the UT carbon-supported film grid (initially suspended in TAEM-2). A diagram of the nanostructure is presented in **Figure 2(b)**. In Rothemund's design, each sharp triangle is formed by three identical trapezoidal domains bridged by staples on their slant faces. *L* represents the major length of a trapezoid formed by 374 bp with a length of ~127 nm (assuming $10.\bar{6}$ bp = 3.63 nm). The width of each trapezoid (t) is $t = 2h + g(h - 1)$, where h is the number of wide helices (9 for a sharp triangle) and g is the inter-helix gap ($g \approx 1$ nm). The calculated width of each side of the triangle is $t = 26$ nm. Based on measurement of ~100 triangles in 5-6 STEM images, the average length *L* was found to be 122.3 ± 6.1 nm, while the average width t was determined at 22.2 ± 2.1 nm. The expected value for the width was calculated assuming the size of free DNA origami triangles in suspension, while the measured value corresponds to dry DNA origami triangles imaged on a carbon substrate. The lack of hydration is likely the source of a slight difference between the measured and calculated sizes. Each of the sharp DNA triangles has a loop in one of the trapezoidal domains formed by a portion of the scaffold not included in the triangle body.[17] Analysis of a random individual triangle, marked with a yellow square in **Figure 2(a)** and digitally zoomed and cropped is

presented in **Figure 2(c),** shows the entangled loop denoted by the red dashed circle. A higher magnification image (*M = 450,000X*) of a single triangle on the UT carbon support is shown in **Figure 2(d)**. Triangles were suspended in TAEM-3 buffer before deposition on the EM grid to provide additional Mg^{2+} cations. Here, fine details of the DNA origami nanostructure can be partially resolved, including the scaffold-to-scaffold distance and the length of the seams in the vertex of a triangle. Rothemund's block diagram of the slant edge of a trapezoidal domain is reproduced in **Figure 2(e)**, where the length of the seam is estimated to be 3 blocks = 10.8 nm (1 block = 3.63 nm).

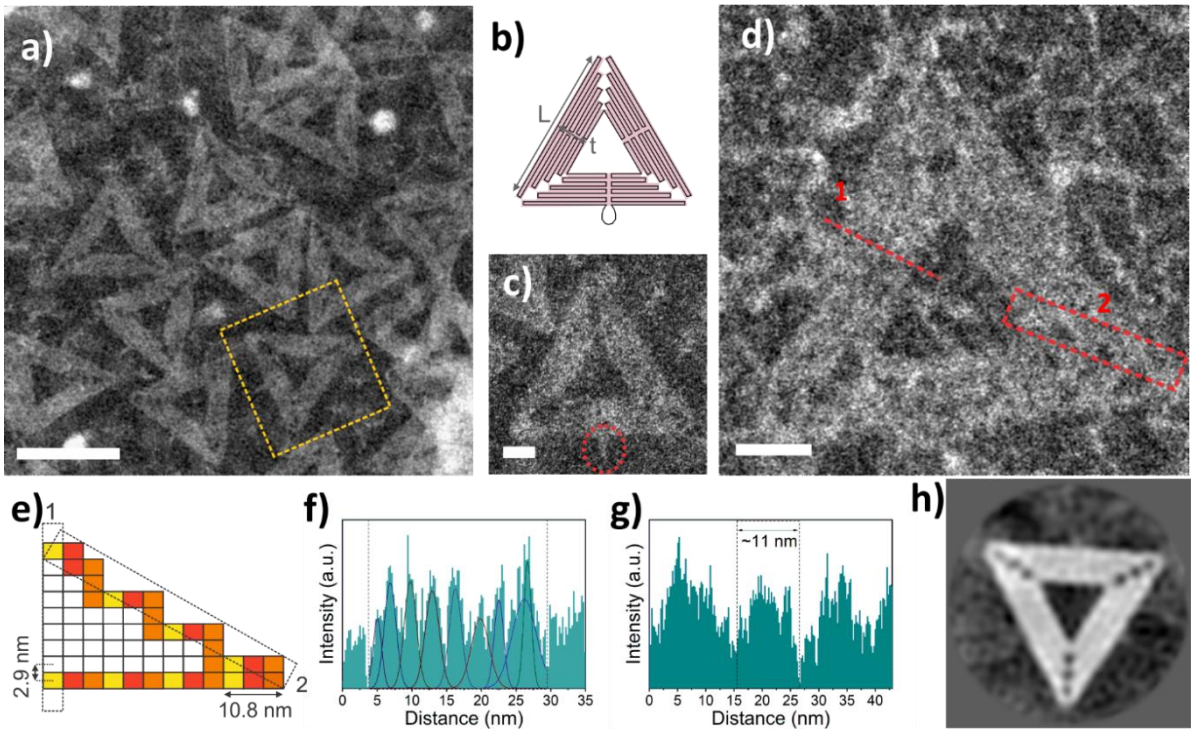

Figure 2. EM imaging of unstained DNA origami triangles. **(a)** HAADF-STEM image of triangles on ultrathin amorphous carbon grids. **(b)** Diagram of the expected structure. **(c)** From the triangle marked with a yellow square in **(a),** the loop formed by the portion of the scaffold not used in the triangle design can be observed (red circle). **(d)** A single triangle can be imaged with sufficient resolution to partially resolve the helices (line 1) as well as the seam length on the scaffold contact along the slant edges (line 2). **(e)** The block diagram of a sharp triangle shows a seam length of 10.8 nm and a scaffold-to-scaffold distance of 2.9 nm. The intensity line profile 1 from the triangle in **(d)** is shown in **(f)** where the 9 helices can be identified along the side of the triangle, using Gaussian functions to model a mean scaffold-to-scaffold distance of ~2.6 nm. Line profile 2 in **(g)** shows an approximate length of seams of 11 nm. **(h)** Representative 2D average from 130 triangles. Scale bar: (a) 100 nm, (c) and (d) 20 nm.

While direct measurement of the distance between helices cannot be realized using the block diagram, because each block includes the inter-helix gap, we can estimate an effective scaffold-to-scaffold distance as the width divided by the number of helices, *i.e.*, $t/9$ (~$2.\bar{8}$ nm). Line 1 drawn across the width of the triangle shown in **Figure 2(d)** was used to gauge the distance between helices. An intensity line profile along this line is shown in **Figure 2(f)**. Using Gaussian functions to fit the intensity of each helix, we can identify the 9 helices forming the short side of the triangle. The average distance between the helices for a group of 4 different triangles fitted with 9 peaks was found to be 2.6 ± 0.2 nm. Our fitted model is similar to the one reported for stained DNA monoliths,[15b] giving a close value to the expected effective width of double helices (~2.4 nm). [15b] The slight difference between measurements taken across the short side of the triangle and the expected scaffold-to-scaffold value was attributed to a decrease of the gap between helices, most likely caused by the dehydration during the sample preparation and EM imaging in the high vacuum environment of the electron microscope. The line profile drawn over the seam on the edge of the triangle in **Figure 2(d)** is presented in **Figure 2(g)** with a mean length value of 11 nm, which is in good agreement with the expected value from the block diagram. Several triangles were used to obtain a 2D average image from a set of 10 low magnification (*M = 110,000X*) images. The class-average image was calculated from 220 triangles classified in 10 classes (see **Figure S3** for details), with the majority of triangles (130) falling in the single class showed in **Figure 2(h)**. The estimated resolution in this class after several cycles of auto refinement in RELION-3[22] converged to a value of 7.8 nm whereas the Fourier Ring Correlation at a threshold of 1/7[23] resulted in a resolution of 9.7 nm (**Figure S3(d)**). In this averaged image the seams are clearly distinguishable, however the individual helices on the side of the triangle are not resolved.

One of the advantages afforded by the EM analysis of DNA origami is the implementation of analytical spectroscopy techniques routinely used in advanced electron microscopes, such as energy-dispersive X-ray spectroscopy (EDS), electron energy loss spectroscopy (EELS) and energy filtering transmission electron microscopy (EFTEM). Use of these techniques, enables probing chemical environment of the DNA origami. An example of elemental mapping obtained by means of energy-filtered transmission electron microscopy is presented and discussed in **Figure S4**.

For AFM characterization, a complete set of experimental variables is available in the literature describing deposition procedures and the effects of substrate, Mg^{2+}, buffer concentration, incubation time, and pH exposure, among others.[1a, 12c, 20, 24] These protocols cannot be directly used with flexible electron transpared susbtrates without further studies. For example, the TAE buffer concentration plays an important role in adhesion of DNA origami structures to a substrate for AFM.[12b, 24b] In our experiments, modifying the TAE buffer concentration used in DNA suspension while keeping the rest of the parameters the same, did not seem to significantly affect the adherence of DNA to the thin carbon substrate, as shown in supporting **Figure S5**. When depositing a specimen from a suspension, we found the hydrophilicity of the carbon substrates played an important role in ensuring DNA adhesion. Supporting **Figure S6** shows successful adhesion to the grids either glow-discharged or UV ozone plasma-cleaned, while non-hydrophilized grids showed no evidence of DNA adhesion.

The image resolution of DNA triangles obtained using HAADF-STEM mode is directly affected by the thickness of the amorphous carbon substrate. Low-scattering substrates with minimum thickness variations are beneficial for enhancing the signal-to-noise-ratio (SNR). It is worth emphasizing, that the resolved structure of DNA origami triangle shown in **Figure 2** was

obtained using a specimen containing a high concentration of Mg^{2+} in the suspension, deposited onto the ultrathin carbon support (< 3 nm). DNA origami triangles have a theoretical height of 2 nm. However, variations in the height as low as ~1 nm have been reported by us[12a] and other groups[11a, 24a, c, 25]. The observed height difference can be associated with a number of experimental parameters, including imaging mode and DNA-surface interactions.[26] The amplitude of the signal in HAADF-STEM mode is sensitive to nanometer-level height fluctuations of the carbon support. We estimated the resolution of the signal by calculating the SNR along the DNA nanostructures. SNR can be calculated as the ratio between the signal and the variation in the background as follows $SNR = {|N_S - N_B|}/{\sigma_B}$ where N_S is the mean value of the signal on a short length of a triangle, while N_B and σ_B are the mean values of the background noise and the standard deviation of the background near a triangle, respectively. Using a DNA nanostructure suspension of 25 ng/μL in TAEM-4; we can calculate the variation in the SNR for DNA origami triangles on different EM substrates. The effect of substrate thickness on the SNR is shown in **Figure 3(a)** for commercially available continuous carbon (CC with a nominal thickness of 15—25 nm),[27] **Figure 3(b)** C-Flat™ grids (CF with a nominal thickness of <20 nm),[28] and **Figure 3(c)** for ultrathin carbon film (UT) on lacey carbon supported Cu grids with mean thickness < 3 nm.[27] It is worth noting, that CF and UT grids are widely used in structural biology experiments for imaging of low-contrast materials.[29]

Area profiles measured across sides of a triangle (marked with dashed red squares) are shown in **Figure 3(d-f)** for the three types of grids used in this study (CC, CF and UT). The intensity profiles for DNA origami triangles on CF and UT films show clear edge distinction between the carbon background and the DNA triangle (uncertainty of the edge is marked with a

rectangular boundary),while DNA origami triangles on the CC film exhibit a broader intensity signal, leading to lower accuracy of detection of clearly resolved edges.

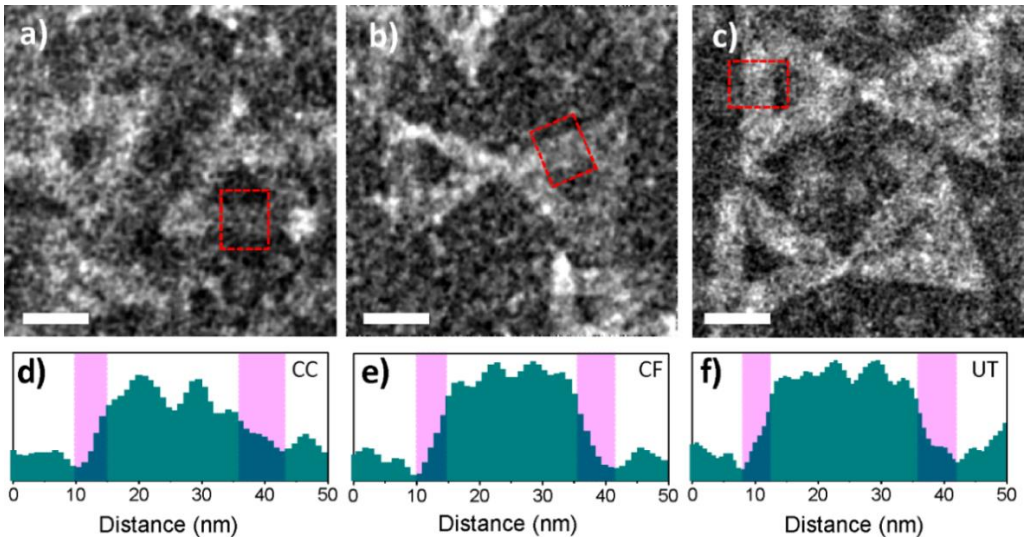

Figure 3. Using the same deposition conditions HAADF-STEM images of DNA triangles have more noise for **(a)** ~ 15-25 nm (nominal thickness) continuous carbon film (CC) grids than for thinner carbon layers as in **(b)** ~ 20 nm C-Flat™ (CF) and **(c)** < 3 nm ultrathin carbon film (UT) on lacey carbon-supported grid. The signal-to-noise ratio can be visualized by the area profile in **(d-e)** for the samples in red squares in **(a-c)**, respectively. Edge detection (rectangular boundaries) improves as the thickness of the substrate decreases. Scale bar: 50 nm.

The SNR calculated for N = 20 line profiles in 6 - 7 triangles is shown in **Table 1**. Each line profile had an average of 30-50 intensity values, from which the mean values of N_S, N_B and σ_B were calculated.

Table 1. Signal-to-noise ratio for N=20 line profiles for DNA origami triangles imaged on three different types of amorphous carbon-based film grids.

Type of grid	**Continuous carbon film (~15-25 nm, nominal thickness, as per the manufacturer)**	**C-Flat™ (~20 nm)**	**Ultrathin carbon film (< 3 nm)**
SNR	2.7 ± 1.7	3.1 ± 0.9	3.0 ± 0.8

The large variation in nominal thickness of the CC film substrate (**Figure 3(a)**), makes it nearly impossible to make a distinction between the DNA signal and carbon background. Following the Rose criterion[30] where the SNR must equal five for 100 % detection of a sharp

object on a flat background, our results indicate that unstained DNA origami nanostructures can be imaged with a 60 % accuracy (SNR = 3) on substrates 3 – 20 times thicker than the DNA. Both CF and UT carbon film grids provided a surface suitable for reliable EM imaging of unstained DNA origami triangles. UT film grids offer a slightly more accurate DNA edge detection (less uncertainty of boundaries) without showing a significant increment in the SNR despise being around 7 times thinner than CF grids. We speculate the reason for this is inherent to the flatness of the substrate: while UT grids provide a higher signal-to-background difference ($|N_S - N_B|$ value), CF provide a lower background variation (lower σ_B).

For semi-flat samples with continuous thickness, in conventional bright-field (BF) TEM the contrast of the image is related to how the sample scatters the incident electrons (diffraction contrast), while in HAADF-STEM the major contribution comes from the electrons scattered at high angles, with the intensity of the same sample sensitive to the atomic number Z and its thickness (the so-called Z-contrast). **Figure 4(a)** shows HAADF-STEM and **Figure 4(b)** BF-TEM images of the same DNA triangle on the UT carbon film obtained by deposition from a suspension of 50 ng/µL DNA in TAEM-3.

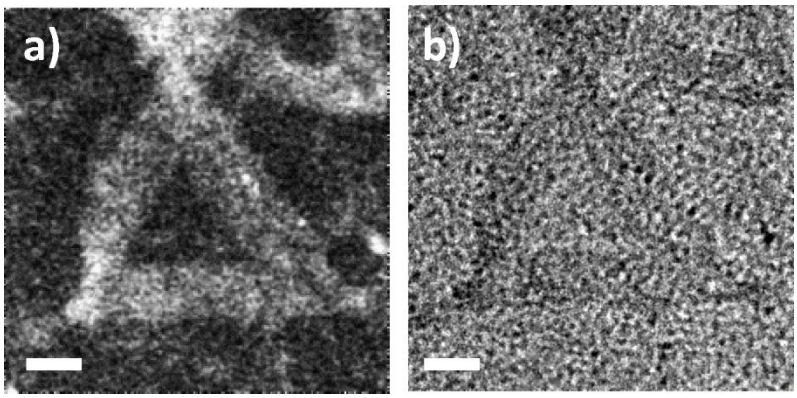

Figure 4. Unstained DNA can be imaged using **(a)** HAADF-STEM and **(b)** BF-TEM modes. The presence of Mg^{2+} provides sufficient Z-contrast to accurately distinguish the DNA nanostructures from the carbon background in **(a)**. The low contrast in BF-TEM provides a high-noise signal making it difficult to resolve the DNA from the background. Scale bar: 20 nm.

Both imaging modes permit differentiation of the triangular shape of the sample from the background. However, the superior image contrast in HAADF-STEM, as compared to the highly defocused BF-TEM, is related to the higher Z-contrast of the DNA-Mg^{2+} triangle immobilized on the carbon background. The analysis of 13-16 line profiles along the short edge of triangles was used to calculated the mean values of $SNR_{HAADF\text{-}STEM}$ = 3.4 ± 0.9 and $SNR_{BF\text{-}TEM}$ = 0.9 ± 0.7. Following the same criteria of SNR equal 5 for 100 % confidence, in BF-TEM mode, the low SNR value indicates that detection of triangles on a carbon substrate is only 20 % accurate.

In the early years of development of DNA imaging, cation-assisted treatment of mica and SiO_2 substrates was initially implemented to immobilize the DNA. Later experiments showed that cation treatment of these substrate was not strictly necessary, as long as sufficient number of cations was available in the buffer to fulfill both adherence and electrostatic screening needs.[31] The threshold of cation content needed to preserve the integrity of the DNA-shaped origami without significantly affecting the density of adhered DNA to a substrate, remains largely unknown. Notably, DNA origami nanostructures are poorly distinguishable from the carbon background when a final concentration of 12.5 mM magnesium acetate (or lower) is used, unless a large supplementary Mg^{2+} is added (as in buffers TAEM 2-4), which generally improves the image contrast of DNA in EM characterization. The results obtained with using a higher Mg^{2+} concentration buffer (not shown) suggest that, by increasing the Mg^{2+} concentration above 12.5 mM, a larger number of divalent cations are available for screening the DNA nanostructure. This, likely, results in enhancement in the EM contrast associated with additional scattering from the surface-residing Mg^{2+}. Excessive amounts of magnesium are often unwanted because these can produce secondary effects in biomedical applications, several attempts to stabilize the DNA nanostructures in Mg^{2+}free or low Mg^{2+} buffers have been reported.[32] We devised a method

alternative to using high (~100 mM) concentrations of $MgCl_2$ in the nanostructure suspension by pre-treating the surface of the negatively charged amorphous carbon with Mg^{2+} cations prior to DNA deposition, in order to enhance DNA adhesion and subsequently, contrast. We explored this possibility by studying the effect of cation-assisted deposition of a suspension of 10 ng/μL DNA origami triangles on the grids on the HAADF-STEM imaging, while keeping the Mg^{2+} concentration constant at 12.5 mM $MgAc_2$ in the TAEM-1 buffer. We chose CF grids instead of UT for this part of this work due to their flatter surface, which helped us achieve a more homogenous spreadability of the suspension without compromising the SNR. Without a cation pre-treatment step on CF grids, the DNA contrast was low. **Figure 5** compares the DNA origami triangle STEM signal as a function of Mg^{2+} treatment of the grids prior to deposition. HAADF-STEM images acquired from the CF girds subject to cationic pre-treatment with 5, 20, 50, and 100 mM aqueous $MgCl_2$ solution prior to DNA origami deposition are shown in **Figure 5(a-d)**, respectively.

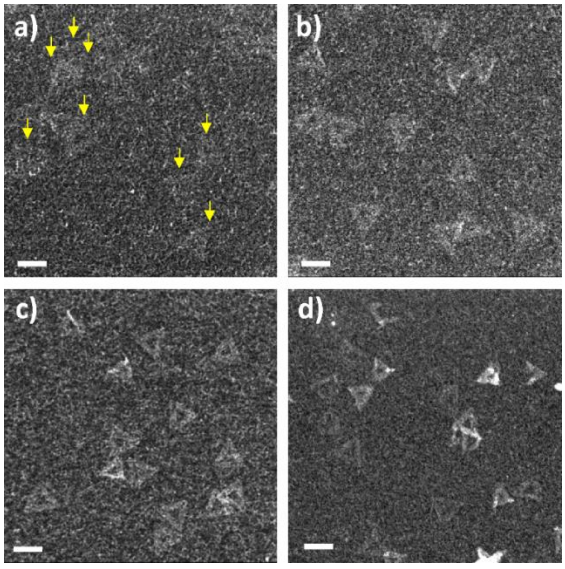

Figure 5. Cationic pre-treatment of the CF grid surface with $MgCl_2$ prior to DNA oriami deposition helps to improve Z-contrast. HAADF-STEM images of substrates treated with **(a)** 5, **(b)** 20, **(c)** 50 and **(d)** 100 mM of $MgCl_2$. Yellow arrows in **(a)** point to the barely visible DNA triangles on a surface treated with 5 mM $MgCl_2$. An increase in the SNR is observed for the CF grids treated with ≥20 mM $MgCl_2$. Scale bar: 100 nm.

Table 2 shows the average SNR for the samples in **Figure 5** plus the case in which no cationic treatment was used (image not shown), for N = 27 - 40 line scans over 7 - 15 triangles for each sample. While the exact mechanism of Mg^{2+} enhancement of DNA contrast in HAADF-STEM imaging is not well understood, the SNR for each case can be used to evaluate contrast quality.

Table 2. Signal-to-noise ratio calculated for N = 27-40 line scans as a function of the $MgCl_2$ concentration used for surface ionic treatment of the grids prior DNA deposition.

$MgCl_2$	**0 mM**	**5 mM**	**20 mM**	**50 mM**	**100 mM**
SNR	2.0 ± 0.9	2.1 ± 0.7	3.5 ± 1.2	2.9 ± 1.0	3.4 ± 1.1

A difference in SNR was observed for the samples in which the substrate was treated with Mg^{2+}. We attribute the observed contrast enhancement to the possible following reasons: 1) during the cationic grid pre-treatment, cations bound to the negatively charged amorphous carbon substrate, form bridges between the negatively bound DNA backbone, becoming essentially trapped beneath the DNA origami triangle surface. These trapped cations contribute to a higher electron scattering density, while the surface-deposited cations not in contact with DNA are washed away when the grid is being rinsed; 2) mixing of the thin layer of $MgCl_2$ remaining after the pretreatment with the DNA origami triangle suspension deposited on carbon grid creates a micro-volume solution with a higher cation concentration during the incubation prior to the grid drying; 3) increased adhesion of DNA triangles resulting in stacking of two or more triangles. Minimal differences in the SNR were observed between conditions that included Mg^{2+}concentrations equal or higher than 20 mM. **Figure 5(d)** shows some brighter triangles with an apparently higher contrast. However, it was observed that the presence of a relatively high Mg^{2+} concentration (100 mM), leads to the aggregation of triangles, with the higher intensity

signal of some triangles attibuted to stacking or distortion of several triangles. We calculated the density of triangles for N = 6 - 7 images within a total area of $\sim 1 - 2\ \mu m^2$, and we found that the density of triangles does not change considerably with the increasing $MgCl_2$ concentrations used for the grid's surface treatment. However, the number of triangles showing distortion in one of the trapezoidal domains, or not lying completely flat on the substrate, is higher for samples suspended in pre-treated grids with 100 mM $MgCl_2$. Further details are discussed in the Supporting Information and presented in **Table S1**.

We wish to point out that that the mechanism of contrast engancement reported here is different from that of commonplace negative staining. In our experiments, the contrast enhancement is brought about by increased cationic bridge formation and larger number of cations effectively trapped between the surface of the grid and DNA triandle (underneath the DNA triangle), while negative staining agent is deposited on over the low-contrast features of interest (on top of the DNA triangle). The location of "high-Z" cations, therefore, is different in both cases, leading to a potential interference from the surface-resisind heavier ions in the event analytical spectroscopy characterization is attempted.

The effective adhesion of DNA origami triangles to pre-treated Mg^{2+} CF grids allows simple visualization of the nanostructures of interest, however it does not permit detecting fine details of the folded scafold presented in the high-resolution image analysis for the case of UT grids. We attribute the increased SNR to the enhancedment in Z-contrast brought about by a cation bridge formed between the negatively-charged DNA backbone, positively charged divalent Mg^{2+} cations, and negatively charged UT grid surface, effectively trapping these under DNA triangles. Further evidence of the Z-contrast dependence in HAADF-STEM images on cation adhesion is shown for CF grids pre-treated with solutions containing four different mono-

and divalent cations. A suspension of 10 ng/μL DNA origami triangles with 12.5 mM $MgAc_2$ in the TAEM-1 buffer was deposited on pre-treated CF grids with 20 mM of the cation, as presented in **Figure 6(a)** for NaCl, **Figure 6(b)** for KCl, **Figure 6(c)** for $MgCl_2$ and **Figure 6(d)** for $BaCl_2$. In **Figure 6**, the cations are arranged in order of increasing *atomic* mass, from light to heavier is Na < Mg < K < Ba. The calculated SNR for a set of N = 20-30 line profiles over the width of the triangles' edge is shown in **Table 3**, lighter to heavier, monovalent to divalent.We attribute the lower SNR found for Na^+ as well as the higher SNR found for Ba^{2+}, to the lower and higher atomic numbers, respectively.

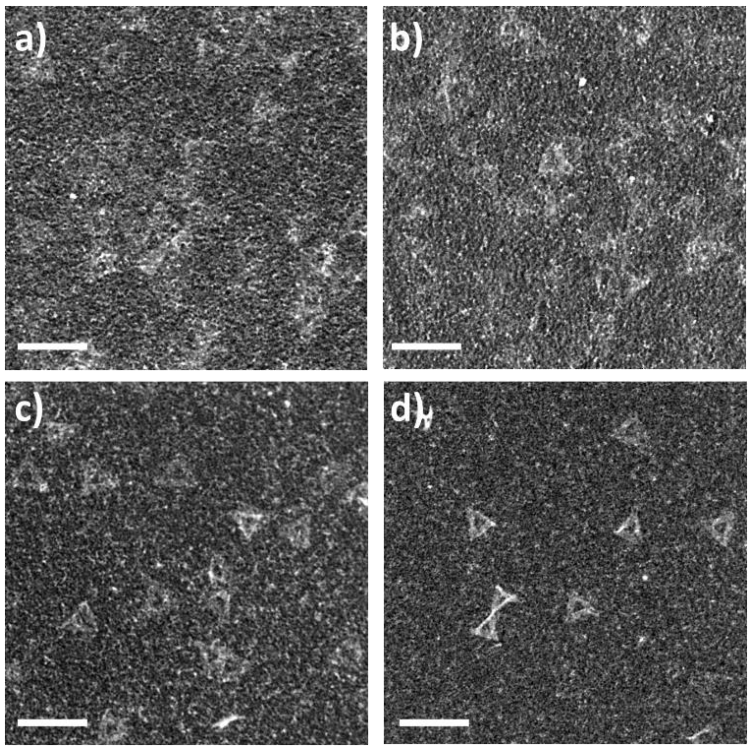

Figure 6. Cation treatment of the grid surface with different cations prior to DNA nanostructure deposition. HAADF-STEM images of substrates treated with 20 mM of **(a)** NaCl, **(b)** KCl, **(c)** $MgCl_2$ and **(d)** $BaCl_2$. The enhanced SNR is related to the atomic number and valence of the cation used to treat the surface of the grid. Scale bar: 200 nm.

At the same time, the enhanced image resolution of the grid pre-treated with Mg^{2+} in comparision with the heavier K^+, is indicative of mono- *vs*. di-valence interplay and point to the

fact that valence of the cation contributes to the amount of "trapped" ions, and therefore, to the final number of cationic bridge atoms contributing to the Z-contrast. These results further reinforce the importance of cations for the succesful visualization of DNA and provide a visual que of the formation of salt bridges betwen pre-treatment cations, surface of the substrate, and the DNA origami.

Table 3. Signal-to-noise ratio calculated for N = 20-30 line scans as a function of the cation used for surface ionic treatment of the grids prior DNA deposition.

	Na^+	K^+	Mg^{2+}	Ba^{2+}
SNR	2.1 ± 0.8	2.5 ± 1.0	3.5 ± 1.2	4.8 ± 1.5

3. Conclusions

We have demonstrated that unstained and visibly intact triangular-shaped DNA can be imaged directly using advanced electron microscopy techniques. Our results showed that HAADF-STEM is suitable to imaging DNA origami nanostructures with spatial resolution adequate for detecting key nanometer-scale structural details and features of interest and also for gauging the stability of these nanostructures, previously only accessible by AFM. We have established a facile preparatory method for depositing DNA origami nanostructures on commercially available thin carbon-supported copper grids and demonstrated how these nanostructures can be visualized with high accuracy. The results and methods reported here do not require elaborate specimen preparation, and instead rely on the immobilization of DNA by ionic bridges on the surface of hydrophilized amorphous carbon films. DNA origami triangles with a nominal height of ~1 nm can be imaged on a variety of EM grids, having enough mass-thickness to provide sufficient Z-contrast on substrates with a nominal thickness up to 25 nm.

Using the Rose criteria, with the accuracy of sample detection defined as 100 % at SNR=5, we observed a decrease in SNR as the substrate's thickness increased up to 25 nm for continuous carbon film grids. We showed that DNA origami nanostructures can also be imaged using conventional BF-TEM, however the edge-detection accuracy and SNR are reduced significantly compared to HAADF-STEM. We discussed an approach alternative to using a high cation concentration in DNA suspension and showed that pre-treating the negatively charged amorphous carbon grids with either a mono- or a divalent cation prior to DNA origami deposition leads to SNR enhancement. We envision our method to be an important milestone in development of electron microscopy-based imaging methods toward comprehensive DNA origami characterization, and we expect our findings to be widely used by researchers working in the field of DNA characterization, offering a straightforward method to high resolution imaging of these nanostructures.

4. Experimental Section

4.1. Materials: All chemicals in this report were used without further modification, unless otherwise noted. Scaffolded DNA (M13mp18) was purchased from Bayou Biolabs (Metairie, LA). Staple oligonucleotides were purchased from Integrated DNA Technologies (Coralville, IA). Mica (Grade V) and silicon substrates were purchased from Structure Probe, Inc. and Ted Pella, respectively. Ultrathin carbon film on lacey carbon supported film, Cu 400 mesh (UT) and continuous carbon support film on Cu 400 mesh grids (CC) were purchased from Ted Pella (Redding, CA). C-Flat^{TM} grids with 1.2 µm holes/1.3 µm space (CF) were purchased from Electron Microscopy Sciences (Hatfield, PA). TAE (40 mM Tris base, 20 mM acetic acid, 1 mM EDTA) buffer (50×) was purchased from Bio-Rad Laboratories (Hercules, CA). Magnesium

chloride (98 %) was purchased from Sigma-Aldrich. Barium chloride dihydrate (>99.0%), potassium chloride (99.0%), and sodium chloride (>99.0%) were purchased from Fisher Chemical. Ultrapure deionized water (18.2 MΩ-cm, 25 °C) was available by Barnstead™ E-Pure™ Ultrapure Water Purification System (Thermo Scientific).

4.2 Synthesis of triangular DNA origami nanostructures: Triangular DNA origami nanostructures were fabricated by annealing 160 nM staples with 16 nM scaffold DNA (10:1 staple to scaffold) in TAE with 12.5 mM $MgAc_2$ (pH 8.3), following Rothemund's published procedure.[17] Annealing was carried out in a MiniOpticon PCR machine (Bio-Rad Laboratories, Hercules, CA) programmed to heat the mixture to 95 °C for 5 min followed by a decrease to 30 °C at a rate of 1 °C min^{-1} in 0.1 °C steps. Following annealing, the excess staples were removed using an Amicon Filter Device (Amicon ultra-0.5 centrifugal filter devices, 100 kDa MWCO). Samples were then transferred to the filter and spun at 14,000 x *g* for 5 min, then the filter was reversed, placed in a fresh tube and spun at 1,500 x *g* for 10 min to collect the purified DNA. Further analysis of DNA suspension was done by diluting the stock solution in the following buffers: TAEM-1 (1×TAE and 12.5 mM $MgAc_2$), TAEM-2 (10×TAE, 0.5 mM $MgAc_2$, 20 mM $MgCl_2$), TAEM-3 (10×TAE, 1 mM $MgAc_2$, 125 mM $MgCl_2$), and TAEM-4 (10×TAE and 0.5 mM $MgAc_2$, 12.5 mM $MgCl_2$).

4.3 Deposition of DNA on mica and silicon: Mica substrates were prepared by cleaving immediately prior to DNA deposition. No further cleaning or surface modification was performed. On freshly cleaved mica, a 2 µL droplet of DNA origami suspension in TAEM-1 was incubated at room temperature for 3-5 min. The mica was then gently rinsed with deionized water and dried under a flow of nitrogen gas. For a silicon surface, an n-type silicon wafer was first cut into pieces and washed with soap water. The Si pieces were then ultrasonicated in

acetone, followed by isopropanol and ultrapure water bath for 10 min each. The chips were finally cleaned by the RCA method to remove any organic and metal contaminants.[21] For this cleaning, the substrates were immersed in a 5:1:1 mixture of H_2O, NH_4OH and H_2O_2 at ~80°C for 15-20 min. The chips were immersed in a second mixture of H_2O, HCl and H_2O_2 at the same temperature for the same 15-20 min period. Afterwards, the silicon wafers were rinsed with deionized water and dried with nitrogen. The cleaned silicon pieces were plasma oxidized in a Harrick Plasma Cleaner (Ithaca, NY) for 10 min. After 2-3 min of plasma oxidation, a 2 µL droplet of DNA origami (50 ng/µL) triangles suspended in 10×TAE buffer with 0.125mM $MgAc_2$ and 125 mM $MgCl_2$ was placed onto the silicon for 5 minutes with a wet Kim wipe placed near the substrate to reduce evaporation of the solution. The silicon substrate was then sequentially rinsed with ethanol/water mixtures corresponding to 90 %, 50 % and 0 % ethanol for 5 sec respectively,[20] followed by drying under a flow of nitrogen between each rinsing step. The dried mica and silicon samples were subsequently used for AFM imaging to verify the deposition of DNA.

4.4 Deposition of DNA on electron transparent substrates: Electron microscopy carbon film grids (ultrathin, pure carbon or C-Flat™) were placed carbon face up on a glass slide and plasma cleaned with UV ozone Procleaner™ (Bioforce Nanosciences, Ames, IA, USA) for 15 min before use, unless otherwise specified. For a typical deposition, suspensions with 50, 25 or 10 ng/µL of DNA were used in TAEM 1-4 respectively as specified. The hydrophilized grids were held with the anti-capillary reverse tweezers and 1 µL of DNA origami suspension was placed on top. The grids were incubated in a closed petri dish for 15 minutes with a wet Kim wipe placed under the grids to prevent evaporation of liquid. The grids were then gently rinsed sequentially with 100 µL of ethanol/water mixtures at 50 % ethanol, 90 % ethanol and finally,

nanopure water.[20] Between each rinse, the grids were dried using a gentle flow of compressed air for 20-30 seconds keeping the flow tangential to the surface of the grids to avoid ripping the carbon film. Ethanol mixtures are commonly used to promote DNA precipitation and improve adhesion to the substrate.[12a, 20, 24a] In our experiments, the grids were rinsed with 50 % ethanol initially to avoid precipitation of salt from the buffer on the surface of the grid. For AFM imaging, an ultrathin carbon film on lacey carbon supported grid was incubated with 1 μL of DNA triangles (10 ng/μL) suspended in TAEM-1. Incubation time and rinsing conditions were the same as described above.

4.5 Cation treatment of electron microscopy grids and DNA deposition: To image the DNA origami triangles suspended in their original TAEM-1 buffer without the addition of extra Mg^{2+} ions, C-Flat™ electron microscope carbon film grids were UV ozone cleaned for 15 min before use. 1 μL of NaCl, KCl, $MgCl_2$ or $BaCl_2$ solution in water (concentration of 5, 20, 50 and 100 mM for $MgCl_2$ and 20 mM for the others cations) was deposited onto the carbon face of the grid and left for 1 min. The excess of liquid was wicked away with lens paper until a thin liquid layer was observed on the grid. After that, 1 μL of DNA origami triangles (10 ng/μL) in TAEM-1 buffer was added to the grid. The grids were incubated with the DNA origami suspension for 15 min and rinsed as described in the previous section.

4.6 Atomic force microscopy (AFM) imaging: Atomic Force Microscope images of the DNA origami nanostructures were obtained using a Dimension 3100 scanning probe microscope in conjunction with a Nanoscope IV controller (Veeco Metrology, LLC, Santa Barbara, CA). Scanning was performed in air with tapping mode using aluminum coated Si tips

(HQ:NSC15/AL BS series, Micromash, Watsonville, CA) with a force constant of ~40 N/m and resonance frequency of ~ 325 kHz.

4.7 Scanning Transmission Electron Microscopy (STEM) imaging: STEM images were recorded using FEI Tecnai G2 F20 microscope equipped with a Tridiem Gatan image filter operating at 200 kV in high angle annular dark field (HAADF) STEM mode working with condenser apertures C1 = 2000 µm and C2 = 70 µm, and a camera length of 87 mm. For all the DNA origami triangles, conventional HAADF-STEM imaging could be performed with a spot size of 5-7. However, all the images reported in this paper were recorded with a spot size 5 to enhance the visual identification of the triangular shape. Over the duration of the experiments, no evidence of induced damage was identified to the nanostructures due to the electron beam. Energy-filtered images were acquired using a 5 mm aperture with an energy dispersion of 0.05 eV/ch and using an exposure time of 10 seconds. Data analysis was performed using DigitalMicrograph® (Gatan) software (version 3.22.1461.0) and Origin® 2018. Unless specified, all images were enhanced by post process filtering. Background noise was reduced by applying a 3x3 low pass filter followed by a smoothing filter to suppress the background noise and enhance the details in the image quality. BF-TEM in **Figure 4** was collected with a spot size 3. For the samples with CF grid pre-treated with cations Na, K, Mg and Ba, in **Figure 6**, acquisition was done in a FEI Titan Themis Cubed operating at 200 kV and working with C1 = 2000 µm, C2 = 50 µm, C3 = 2000 µm and a camera length of 145 mm in spot size 9 with a beam current of 100 pA.

4.8 Image 2D average: A set of ten images with calibrated pixel of 9.4 Å were converted from dm4 format to mrc using IMOD 4.8.[33] Triangles were picked from images using

EMAN2[34] e2boxer.py routine under Swarm mode and manually supervised for accuracy of selection. A total of 220 triangles were chosen. Extraction, normalization, and reference-free 2D class averaging were done in RELION-3.0[22] with several auto-refine iterations until estimated resolution converged to a minimum. The Fourier Ring Correlation was obtained in ImageJ with an FRC plugin.[35]

Conflict of Interest

The authors declare no conflict of interest.

Supporting Information

Supporting Information is available from the Wiley Online Library or at https://doi.org/10.25380/iastate.7800956.v1

Research Data for this Article

The datasets generated and analyzed for this study can be found at https://doi.org/10.25380/iastate.7800956.v1

Acknowledgements

This work was supported by the U.S. Department of Energy (DOE), Office of Science, Basic Energy Sciences, Materials Sciences and Engineering Division. The research was performed at the Ames Laboratory, which is operated for the U.S. Department of Energy by Iowa State University under Contract No. DE-AC02-07CH11358. All electron microscopy

imaging was performed using instruments in the Sensitive Instrument Facility in Ames Laboratory.

Received: ((will be filled in by the editorial staff))
Revised: ((will be filled in by the editorial staff))
Published online: ((will be filled in by the editorial staff))

References

[1] a) S. Ramakrishnan, H. Ijäs, V. Linko and A. Keller, *Computational and Structural Biotechnology Journal* **2018**, *16*, 342-349; b) D. Jiang, C. G. England and W. Cai, *Journal of controlled release : official journal of the Controlled Release Society* **2016**, *239*, 27-38; c) Y. Zhang, J. Tu, D. Wang, H. Zhu, S. K. Maity, X. Qu, B. Bogaert, H. Pei and H. Zhang, *Advanced Materials* **2018**, *30*, 1703658; d) B. Zhu, L. Wang, J. Li and C. Fan, *The Chemical Record* **2017**, *17*, 1213-1230; e) A. H. Okholm and J. Kjems, *Advanced Drug Delivery Reviews* **2016**, *106*, 183-191; f) K.-R. Kim, H. Y. Kim, Y.-D. Lee, J. S. Ha, J. H. Kang, H. Jeong, D. Bang, Y. T. Ko, S. Kim, H. Lee and D.-R. Ahn, *Journal of Controlled Release* **2016**, *243*, 121-131.

[2] a) Y. Huang, M.-K. Nguyen, A. K. Natarajan, V. H. Nguyen and A. Kuzyk, *ACS Applied Materials & Interfaces* **2018**, *10*, 44221-44225; b) D. Daems, W. Pfeifer, I. Rutten, B. Saccà, D. Spasic and J. Lammertyn, *ACS Applied Materials & Interfaces* **2018**, *10*, 23539-23547; c) D. Selnihhin, S. M. Sparvath, S. Preus, V. Birkedal and E. S. Andersen, *ACS Nano* **2018**, *12*, 5699-5708; d) E. A. Hemmig, C. Fitzgerald, C. Maffeo, L. Hecker, S. E. Ochmann, A. Aksimentiev, P. Tinnefeld and U. F. Keyser, *Nano Letters* **2018**, *18*, 1962-1971.

[3] a) F. Hong, F. Zhang, Y. Liu and H. Yan, *Chemical Reviews* **2017**, *117*, 12584-12640; b) J. Chao, Y. Lin, H. Liu, L. Wang and C. Fan, *Materials Today* **2015**, *18*, 326-335; c) M. J. Urban, P. K. Dutta, P. Wang, X. Duan, X. Shen, B. Ding, Y. Ke and N. Liu, *Journal of the American Chemical Society* **2016**, *138*, 5495-5498; d) C. Zhu, M. Wang, J. Dong, C. Zhou and Q. Wang, *Langmuir* **2018**, *34*, 14963-14968; e) X. Lan, T. Liu, Z. Wang, A. O. Govorov, H. Yan and Y. Liu, *Journal of the American Chemical Society* **2018**, *140*, 11763-11770.

[4] a) Z. Chen, C. Liu, F. Cao, J. Ren and X. Qu, *Chemical Society Reviews* **2018**, *47*, 4017-4072; b) P. Wang, T. A. Meyer, V. Pan, P. K. Dutta and Y. Ke, *Chem* **2017**, *2*, 359-382.

[5] S. Nummelin, J. Kommeri, M. A. Kostiainen and V. Linko, *Advanced Materials* **2018**, *30*, 1703721.

[6] A. Xu, J. N. Harb, M. A. Kostiainen, W. L. Hughes, A. T. Woolley, H. Liu and A. Gopinath, *MRS Bulletin* **2017**, *42*, 943-950.

[7] H. Wang, Y. Yang and D. A. Erie in *Characterization of Protein–Protein Interactions Using Atomic Force Microscopy*, (Ed. P. Schuck), Springer US, Boston, MA, **2007**, pp. 39-77.

[8] Y. L. Lyubchenko, *Micron* **2011**, *42*, 196-206.

[9] a) D. Alloyeau, B. Ding, Q. Ramasse, C. Kisielowski, Z. Lee and K.-J. Jeon, *Chemical Communications* **2011**, *47*, 9375-9377; b) X. Liu, F. Zhang, X. Jing, M. Pan, P. Liu, W. Li, B. Zhu, J. Li, H. Chen, L. Wang, J. Lin, Y. Liu, D. Zhao, H. Yan and C. Fan, *Nature* **2018**, *559*, 593-598.

[10] C. Brack, *CRC Crit Rev Biochem* **1981**, *10*, 113-169.

[11] a) C. Bustamante, J. Vesenka, C. L. Tang, W. Rees, M. Guthold and R. Keller, *Biochemistry* **1992**, *31*, 22-26; b) J. Vesenka, M. Guthold, C. L. Tang, D. Keller, E. Delaine and C. Bustamante, *Ultramicroscopy* **1992**, *42-44*, 1243-1249.

[12] a) M. M. Hossen, L. Bendickson, P. E. Palo, Z. Yao, M. Nilsen-Hamilton and A. C. Hillier, *Nanotechnology* **2018**, *29*, 355603; b) R. J. Kershner, L. D. Bozano, C. M. Micheel, A. M. Hung, A. R. Fornof, J. N. Cha, C. T. Rettner, M. Bersani, J. Frommer, P. W. K. Rothemund and G. M. Wallraff, *Nature Nanotechnology* **2009**, *4*, 557; c) K. B. Ricardo, A. Xu, M. Salim, F. Zhou and H. Liu, *Langmuir* **2017**, *33*, 3991-3997.

[13] J. Zheng, Z. Li, A. Wu and H. Zhou, *Biophysical Chemistry* **2003**, *104*, 37-43.

[14] a) X.-c. Bai, T. G. Martin, S. H. W. Scheres and H. Dietz, *Proceedings of the National Academy of Sciences* **2012**, *109*, 20012; b) T. G. Martin, T. A. M. Bharat, A. C. Joerger, X.-c. Bai, F. Praetorius, A. R. Fersht, H. Dietz and S. H. W. Scheres, *Proceedings of the National Academy of Sciences* **2016**, *113*, E7456; c) D. Lei, A. E. Marras, J. Liu, C.-M. Huang, L. Zhou, C. E. Castro, H.-J. Su and G. Ren, *Nature Communications* **2018**, *9*, 592.

[15] a) H. Dietz, S. M. Douglas and W. M. Shih, *Science* **2009**, *325*, 725; b) S. M. Douglas, H. Dietz, T. Liedl, B. Högberg, F. Graf and W. M. Shih, *Nature* **2009**, *459*, 414; c) Y. Kabiri, A. Angelin, I. Ahmed, H. Mutlu, J. Bauer, C. M. Niemeyer, H. Zandbergen and C. Dekker,

ChemBioChem **2018**, *0*; d) C. Plesa, A. N. Ananth, V. Linko, C. Gülcher, A. J. Katan, H. Dietz and C. Dekker, *ACS Nano* **2014**, *8*, 35-43.

[16] a) M. Marini, A. Falqui, M. Moretti, T. Limongi, M. Allione, A. Genovese, S. Lopatin, L. Tirinato, G. Das, B. Torre, A. Giugni, F. Gentile, P. Candeloro and E. Di Fabrizio, *Science Advances* **2015**, *1*, e1500734; b) M. Marini, M. Allione, S. Lopatin, M. Moretti, A. Giugni, B. Torre and E. di Fabrizio, *Microelectronic Engineering* **2018**, *187-188*, 39-42; c) F. Gentile, M. Moretti, T. Limongi, A. Falqui, G. Bertoni, A. Scarpellini, S. Santoriello, L. Maragliano, R. Proietti Zaccaria and E. di Fabrizio, *Nano Letters* **2012**, *12*, 6453-6458.

[17] P. W. K. Rothemund, *Nature* **2006**, *440*, 297.

[18] a) Y. Kabiri, A. N. Ananth, J. van der Torre, A. Katan, J.-Y. Hong, S. Malladi, J. Kong, H. Zandbergen and C. Dekker, *Small* **2017**, *13*, 1700876; b) S. Buckhout-White, J. T. Robinson, N. D. Bassim, E. R. Goldman, I. L. Medintz and M. G. Ancona, *Soft Matter* **2013**, *9*, 1414-1417; c) T. H. Brintlinger, N. D. Bassim, R. M. Stroud, J. T. Robinson, S. Buckhout-White, M. Ancona and E. Goldman, *Microscopy and Microanalysis* **2018**, *24*, 386-387.

[19] Y. L. Lyubchenko, L. S. Shlyakhtenko and T. Ando, *Methods* **2011**, *54*, 274-283.

[20] A. Gopinath and P. W. K. Rothemund, *ACS Nano* **2014**, *8*, 12030-12040.

[21] W. Kern, *Journal of The Electrochemical Society* **1990**, *137*, 1887-1892.

[22] J. Zivanov, T. Nakane, B. O. Forsberg, D. Kimanius, W. J. H. Hagen, E. Lindahl and S. H. W. Scheres, *eLife* **2018**, *7*, e42166.

[23] a) P. B. Rosenthal and R. Henderson, *Journal of Molecular Biology* **2003**, *333*, 721-745; b) M. van Heel and M. Schatz, *Journal of Structural Biology* **2005**, *151*, 250-262.

[24] a) H. Kim, S. P. Surwade, A. Powell, C. O'Donnell and H. Liu, *Chemistry of Materials* **2014**, *26*, 5265-5273; b) K. Brassat, S. Ramakrishnan, J. Bürger, M. Hanke, M. Doostdar, J. K. N. Lindner, G. Grundmeier and A. Keller, *Langmuir* **2018**, *34*, 14757-14765; c) M. Rahman, D. Neff, N. Green and M. L. Norton, *Nanomaterials (Basel, Switzerland)* **2016**, *6*, 196; d) S. Takabayashi, S. Kotani, J. Flores-Estrada, E. Spears, E. J. Padilla, C. L. Godwin, E. Graugnard, W. Kuang, S. Sills and L. W. Hughes, *International Journal of Molecular Sciences* **2018**, *19*, 2513; e) M. A. Pillers, R. Shute, A. Farchone, K. P. Linder, R. Doerfler, C. Gavin, V. Goss and M. Lieberman, *Journal of visualized experiments : JoVE* **2015**,

e52972-e52972; f) Y. Chen, P. Wang, Y. Liu, T. Liu, Y. Xu, S. Zhu, J. Zhu, K. Ye, G. Huang and H. Dannong, *Nanotechnology* **2017**, *29*, 035102.

[25] S. P. Surwade, S. Zhao and H. Liu, *Journal of the American Chemical Society* **2011**, *133*, 11868-11871.

[26] F. Moreno-Herrero, J. Colchero and A. M. Baró, *Ultramicroscopy* **2003**, *96*, 167-174.

[27] Ted Pella Inc., https://www.tedpella.com/, accessed: 02/28/2019

[28] Electron Microscopy Sciences, https://www.emsdiasum.com/, accessed: 02/28/2019

[29] a) X. Zhang, E. Settembre, C. Xu, P. R. Dormitzer, R. Bellamy, S. C. Harrison and N. Grigorieff, *Proceedings of the National Academy of Sciences* **2008**, *105*, 1867; b) M. A. Schumacher, T. C. Glover, A. J. Brzoska, S. O. Jensen, T. D. Dunham, R. A. Skurray and N. Firth, *Nature* **2007**, *450*, 1268.

[30] A. Rose, *Vision : Human and Electronic*, Plenum Press, New York, **1974**

[31] M. Bezanilla, S. Manne, D. E. Laney, Y. L. Lyubchenko and H. G. Hansma, *Langmuir* **1995**, *11*, 655-659.

[32] a) T. G. Martin and H. Dietz, *Nature Communications* **2012**, *3*, 1103; b) C. Kielar, Y. Xin, B. Shen, M. A. Kostiainen, G. Grundmeier, V. Linko and A. Keller, *Angewandte Chemie International Edition* **2018**, *57*, 9470-9474; c) H. Auvinen, H. Zhang, Nonappa, A. Kopilow, E. H. Niemelä, S. Nummelin, A. Correia, H. A. Santos, V. Linko and M. A. Kostiainen, *Advanced Healthcare Materials* **2017**, *6*, 1700692; d) N. Ponnuswamy, M. M. C. Bastings, B. Nathwani, J. H. Ryu, L. Y. T. Chou, M. Vinther, W. A. Li, F. M. Anastassacos, D. J. Mooney and W. M. Shih, *Nature Communications* **2017**, *8*, 15654; e) Y. Ahmadi and I. Barisic, *JoVE* **2019**, e58771; f) D. Zhang and P. J. Paukstelis, *ChemBioChem* **2016**, *17*, 1163-1170.

[33] J. R. Kremer, D. N. Mastronarde and J. R. McIntosh, *Journal of Structural Biology* **1996**, *116*, 71-76.

[34] G. Tang, L. Peng, P. R. Baldwin, D. S. Mann, W. Jiang, I. Rees and S. J. Ludtke, *Journal of Structural Biology* **2007**, *157*, 38-46.

[35] R. P. J. Nieuwenhuizen, K. A. Lidke, M. Bates, D. L. Puig, D. Grünwald, S. Stallinga and B. Rieger, *Nature Methods* **2013**, *10*, 557.

Table of contents

Imaging of Unstained DNA Origami Triangles with Electron Microscopy

Alejandra Londono-Calderon, Md Mir Hossen, Pierre E. Palo, Lee Bendickson, Sandra Vergara, Marit Nilsen-Hamilton, Andrew C. Hillier and Tanya Prozorov*

Direct imaging of visibly intact DNA origami triangles with Scanning Transmission Electron Microscopy is presented. DNA is deposited on commercially available electron microscopy grids and imaged in HAADF-STEM mode without the use of staining agent. The signal-to-noise ratio of the DNA triangles on an ultrathin carbon substrate is sufficient to resolve the scaffold-to-scaffold distance in the triangle's design.

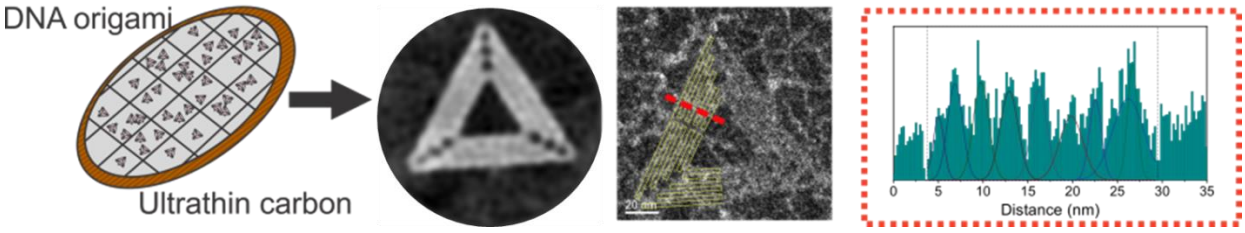

Keyword: unstained DNA origami imaging